An Ingestible Sensor for Measuring Medication Adherence

Hooman Hafezi, Timothy L. Robertson*, *Member, IEEE*, Greg D. Moon, Kit-Yee Au-Yeung, Mark J. Zdeblick, *Member, IEEE*, and George M. Savage

***Abstract*—In this paper, we describe the design and performance of the first integrated-circuit microsensor developed for daily ingestion by patients. The ingestible sensor is a device that allows patients, families, and physicians to measure medication ingestion and adherence patterns in real time, relate pharmaceutical compliance to important physiologic metrics, and take appropriate action in response to a patient's adherence pattern and specific health metrics. The design and theory of operation of the device are presented, along with key *in-vitro* and *in-vivo* performance results. The chemical, toxicological, mechanical, and electrical safety tests performed to establish the device's safety profile are described in detail. Finally, aggregate results from multiple clinical trials involving 412 patients and 5656 days of system usage are presented to demonstrate the device's reliability and performance as part of an overall digital health feedback system.**

***Index Terms*—Electrochemical devices, galvanic coupling, gastrointestinal fluid, human body tissues, intra-body networks, pharmaceutical adherence, sensor, wireless communication.**

I. Introduction

DIGITAL medicine—the use of wearable and implantable physiological sensors, mobile communication technology, and web-based patient communities in managing patient health—represents a new and rapidly evolving paradigm in healthcare. Continuous measurement of physiological metrics and rapid sharing of data between patients and caregivers offers unprecedented opportunities for diagnosing disease, tailoring treatment to individual patient physiology and behavior, and responding to new information with little or no delay. These capabilities can provide solutions to some of the most elusive and intractable challenges in healthcare.

Medication nonadherence is one such problem. Recent studies have estimated that 30–50% of drug prescriptions are never taken [1]–[3], resulting in significant complications and deterioration of patient health [4], [5]. In 2009, the estimated economic cost of nonadherence in the U.S.—including wasted drugs, treatment of complications, and hospitalizations—was nearly equal to the total spending on prescription drugs—$289B [2] versus $301B [6]. The extent and impact of the problem are expected to grow as patients live longer lives, often requiring management of one or more chronic conditions with multiple medications.

Fig. 1 Proteus Digital Health Feedback System—the system consists of ingestible sensors embedded in tablets, a skin-worn receiver patch, and a mobile device based user interface.

In this paper, we present a novel sensor for detecting the ingestion of a pharmaceutical tablet or capsule. The microfabricated sensor is designed to be incorporated into every "digital" tablet or capsule during pharmaceutical manufacturing. Upon ingestion and contact with the fluid in the stomach, each sensor communicates a unique and private digital code to identify the medication and dose. In combination with a wearable sensor patch and a mobile-phone-based user interface (see Fig. 1), the sensor provides a system for real-time, continuous measurement of medication adherence. The system further allows direct correlation between drug ingestion, health-related behaviors such as physical activity, and critical metrics of physiological response, such as heart rate, sleep quality, and blood pressure. The ingestible sensor and digital health feedback system have received regulatory approval from the Food and Drug Administration [7] in the U.S. and CE Mark designation in Europe.

We begin with a discussion of the sensor design and theory of operation. Results from *in vitro* tests, finite-element simulations, and clinical and preclinical studies are discussed to highlight the key factors involved in sensor operation and detection. Of particular importance is the sensor's ability to function in a wide range of fluids that may be present in the stomach. A series of clinical studies have been performed since 2008, comprising 20 000+ device ingestions. The results of these studies are reviewed in terms of sensor performance and safety.

Manuscript received December 2, 2013; revised March 11, 2014; accepted April 9, 2014. Date of publication July 21, 2014; date of current version December 18, 2014. *Asterisk indicates corresponding author*

H. Hafezi was with Proteus Digital Health, Redwood City, CA 94065 USA. He is now with Nernst Engineering, Redwood City, CA 94065 USA (e-mail: HH@NERNST.NET).

K.-Y. Au-Yeung was with Proteus Digital Health, Redwood City, CA 94065 USA. She is now with Profusa Corporation, San Francisco, CA 94107 USA (e-mail: kauyeung@proteusdh.com).

*T. L Robertson was with Proteus Digital Health, Redwood City, CA 94065 USA. He is now with Mousera, Inc., Belmont, CA 94002 USA (e-mail: timothyr@timothyr.org).

G. D. Moon, M. J. Zdeblick, and G. M. Savage are with Proteus Digital Health, Redwood City, CA 94065 USA (e-mail: gmoon@proteusdh.com; mzdeblick@proteusdh.com; gsavage@proteusdh.com).

Digital Object Identifier 10.1109/TBME.2014.2341272

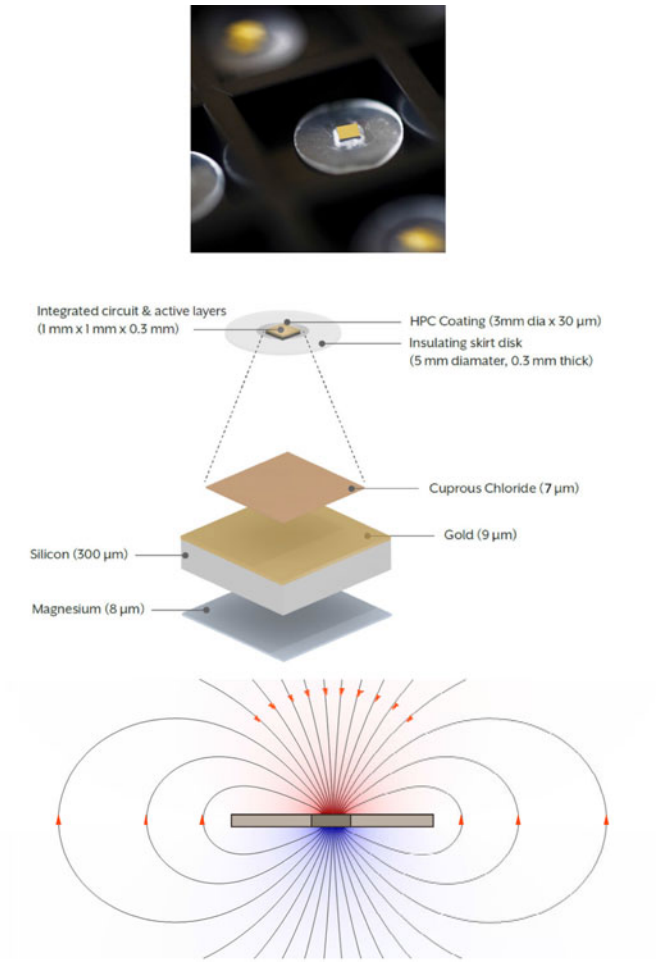

Fig. 2 Photograph and schematic of the ingestible sensor and cross-section showing electric potential and current flow (arrows) around the sensor.

Safety was a critical consideration in developing the sensor, which represents the first instance of a microfabricated device developed and commercialized for daily ingestion. The safety considerations and evaluations are presented and discussed in detail. Together with the sensor's performance in clinical trials, these results demonstrate that the device is a safe and reliable tool for measuring medication adherence.

II. System Design

A. Design and Principle of Operation

The sensor (see Fig. 2) consists of three functional components: 1) the active layers, 2) the integrated circuit (IC), and 3) the insulating skirt disk. The integrated circuit is a food-particle sized 1 mm $\times$ 1 mm $\times$ 0.3 mm CMOS chip. After production of the IC, the active layers are deposited directly on the silicon wafers using a sequence of microfabrication steps. This begins with the deposition by evaporation of 8 μm of magnesium on the substrate side of the wafer. Afterward, using shadow masks to define deposition areas, 9 μm of Gold is deposited by evaporation over the integrated circuit side of the wafer. Next, again using shadow masks, 7 μm of Cuprous Chloride is deposited on top of the gold underlayer. The wafers are then singulated using a laser scribe. The individual ICs are placed into a previously punched hole in a sheet of skirt material using a pick-and-place machine, then attached to the skirt material using an edible adhesive material. The final round skirt is formed using a punch, releasing the individual sensors which are then secured to an IC-industry-standard reel that holds thousands of completed sensors. These reels of ingestible sensors are delivered to a semicustom pharmaceutical press, where an ingestion sensor is inserted into each die along with the pharmaceutical powder that is then pressed into a tablet.

Each component of the sensor provides a specific function. The active layers are thin films of magnesium and cuprous chloride. The gold underlayer acts as current collector underneath the cuprous chloride. Upon contact with gastric fluid, these layers create a battery that activates and powers the device. The following electrode reactions are initiated as soon as the electrolytic fluid in the stomach creates a continuous conductive path between the anode (Mg) and cathode (CuCl):

$$\text{Anode: } \mathrm{Mg(s)} \rightarrow \mathrm{Mg^{2+}(aq)} + 2\mathrm{e^-} \tag{1}$$

$$\text{Cathode: } \mathrm{CuCl(s)} + \mathrm{e^-} \rightarrow \mathrm{Cu(s)} + \mathrm{Cl^-(aq)} \tag{2}$$

$$\text{Overall: } \mathrm{Mg(s)} + 2\mathrm{CuCl(s)} \rightarrow 2\mathrm{Cu(s)} + 2\mathrm{Cl^-} + \mathrm{Mg^{2+}(aq)}. \tag{3}$$

The theoretical open circuit voltage (E_o) of the overall reaction is 2.5 V. In aqueous solution however, the maximum observed open circuit potential is 1.85 V, due to a side reaction that occurs on the magnesium electrode and reduces the available voltage

$$\mathrm{Mg\,(s)} + 2\mathrm{H_2O(l)} \rightarrow \mathrm{Mg(OH)_2\,(s)} + \mathrm{H_2\,(g)}. \tag{4}$$

The electrode materials are the same as those used in magnesium reserve batteries [8], [9]. Other electrode materials have been previously proposed for powering devices using physiological fluids as electrolyte [10], [11]; however, the Mg/CuCl pair provides an optimum combination of biocompatibility, power, compatibility with microfabrication processes, and cost. Once activated, reactions (1)–(3) proceed at a rate equal to the current flow through the IC. Copper is deposited on the cathode and is gradually converted to copper oxide, which gradually dissolves to release Cu^{2+} ions as the device travels through the GI tract. Mg^{2+} ions are released at the anode through reaction (2) as well as the slow dissolution of $Mg(OH)_2$ from reaction (4). The quantities of various materials released to the body are extremely low compared to the levels commonly present in the GI tract or ingested as part of a typical diet. This is discussed in detail in the safety and toxicology section.

The electrochemical reactions continue until the electrode materials are exhausted. The duration of discharge depends on both the amount of active material on the sensor (7 μm CuCl, 8 μm Mg) and the conductivity of the fluid environment around the device. *In vivo*, the fluid conductivity is variable and depends on gastric secretions and the composition of food or medication ingested with the sensor. The sensor must function over the full range of such solutions that define the device's impedance, output current, and discharge lifetime. Typical *in-vivo* values of

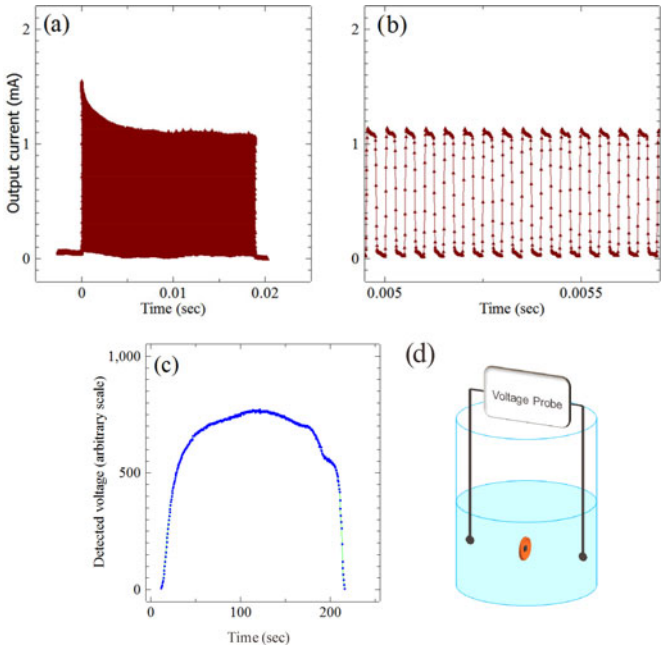

Fig. 3 Output from a typical sensor in a benchtop test cell using a saline solution at 7 mS/cm and 37 °C. A data packet (a) consists of a sequence of low and high current pulses (b). Packets are detected as voltage differences (c) between a pair of receiver electrodes in the test cell (d). Each dot in Fig. 3 (c) is due to one data packet. A device transmits hundreds of packets over its discharge life.

average discharge current and lifetime are 0.1 mA and 4 min, respectively.

The flow of current produced by reactions (1)–(3) generates an electric field similar in shape to that of an electric dipole (two electrostatic charges or potentials separated by a finite separation) (see Fig. 2). The electric field is shaped by the insulating skirt, propagates through the surrounding tissue, and is detected on the skin by a wearable voltage probe or receiver. This electric field is similar in nature to the electrophysiological signals generated by the brain, heart, and gastrointestinal tract. The code transmitted by the device consists of a binary number that represents the medication and dose of interest. The code is stored in the nonvolatile memory of the IC. To transmit the code, the IC modulates the discharge current between high ($\sim$1 mA) and low ($<$20 μA) levels. Data packets are transmitted approximately twice a second at several frequencies between 10 and 30 kHz. The frequencies were chosen to avoid interference from common medical instruments, consumer electronic devices, and the electrophysiological signals of the body which are typically between 10–100 Hz. These frequencies further ensure that the electric signal does not stimulate any cells or tissue as discussed in the electrical safety section.

A typical data packet is shown in Fig. 3(a) and (b). The current pulses generated by the sensor result in a voltage difference between a pair of electrodes immersed in the test beaker [see Fig. 3(d)] or on a skin-worn or implanted receiver unit. The detected voltage is directly proportional to the current output, but its exact value depends on the position of the receiver electrodes relative to the sensor and the size of the test cell. Hence, the voltage axis in Fig. 3(c) is shown as an arbitrary axis that depends on the test cell configuration, while the current output [see Fig. 3(a) and (b)] depends only on solution conductivity and device impedance and is thus unambiguous. The output currents in Fig. 3 provide *in-vivo* signals of up to 150 μV at the wearable receiver, although this value again depends somewhat on the choice and location of receiver system. These effects are discussed in detail in the following section.

B. Signal Propagation in the Body

Besides the integrated circuit and active layers, the third component of the sensor is the insulating "skirt" disk. The function of the skirt is to shape and amplify the electric field generated by the sensor. To see this, it is helpful to start with the theoretical expression for the potential surrounding a dipole in a conductive sphere [12]. For a dipole with current I and length d, located at the center of a sphere of radius R and conductivity κ, the voltage on the sphere surface is given by

$$\mathrm{V} = 3Id\cos\theta/4\,\pi\kappa\mathrm{R}^2 \tag{5}$$

and the voltage difference between two probes on the surface is

$$\Delta\mathrm{V} = 3Id/4\,\pi\kappa\mathrm{R}^2(\cos\theta_1 - \cos\theta_2). \tag{6}$$

In (5), θ is the angle between the dipole vector and the measurement location on the sphere. For a vertically oriented dipole, $\theta = 0°$ at the top of the sphere and 90° in the plane of the equator.

The addition of the skirt extends the current path and increases V and ΔV in a similar fashion to increasing d. Fig. 4(a) shows benchtop measurements (symbols) and finite element simulations (lines) of signals due to sensors of varying skirt size. The simulations and benchtop results agree well and show that the detected signal is indeed proportional to skirt radius. Fig. 4(a) also shows simulations of dipoles of varying lengths without a skirt (blue line). Comparison of the two lines shows the effect of the skirt. For example, a 0.3-mm long dipole with a 2.5-mm radius skirt generates a signal equal to a 1.9-mm-long dipole without skirt, a $\sim$6$\times$ improvement in amplitude.

The skirt is made of standard pharmaceutical excipients (ethyl cellulose, hydroxypropyl cellulose, and triethyl citrate) and is a critical part of the sensor design. By enhancing the signal amplitude, the skirt allows the sensor to be only 300 μm thick. This makes it feasible to manufacture the device almost entirely on a silicon wafer without the need for extended electrical antennas and connections. More importantly, it allows the rigid part of the device to be very small—the size of a small food particle—which ensures facile passage through the GI tract.

Equation (6) shows the other key parameters that influence the detected signal. These include the conductivity of the torso κ, the distance between the sensor and the receiver R (equivalent to the size of the patient), and the current output of the device. Current output is a function of the device's voltage and impedance. The latter depends strongly on the conductivity of the gastric medium. Gastric fluid has a conductivity that is approximately 10$\times$ that of the rest of the torso (see Table I). This difference in conductivity has an important impact on the detected signal. This can be seen with a modified form of (5) derived for a sphere

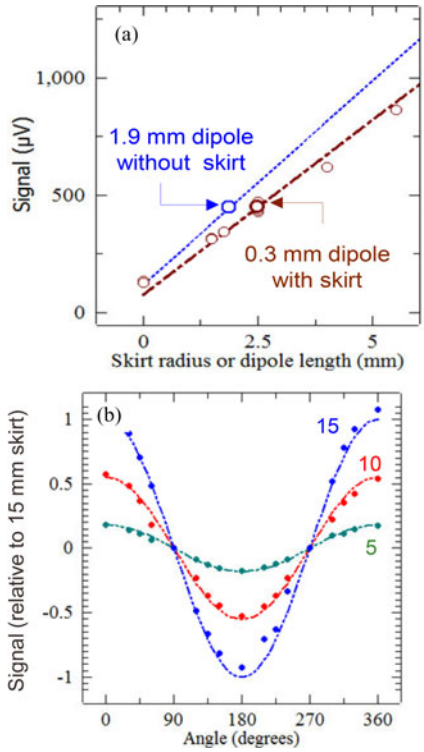

Fig. 4 Effect of skirt size on signal strength shown in terms of (a) average detected signal over device lifetime and (b) relative signal strength as a function of angle between receiver and the device in the setup shown in Fig. 3(d). Experimental data (symbols) and finite elements (lines) simulations show good agreement. The different curves in 4b are for skirt radii of 5, 10, and 15 mm, respectively.

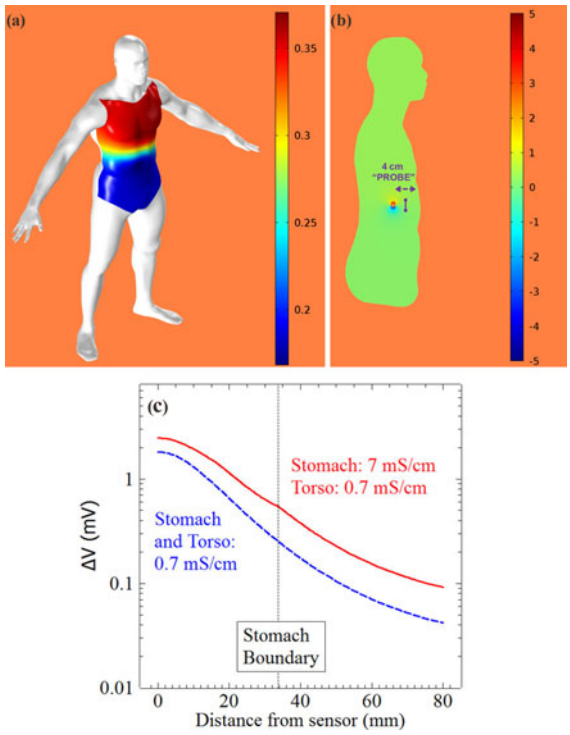

Fig. 5 Finite element simulations of the sensor signal (a) Potential (mV) on the skin surface. (b) Potential (mV) inside the body. (c) Potential difference (mV) measured by the imaginary 4 cm probe shown in (b) as it is moved away from the device. The voltages shown in (a) and (b) are relative to the center of the sensor, which is taken as the arbitrary zero of potential. The two curves in (c) compare the signal with a uniform conductivity in the body versus a stomach with 10× higher conductivity than the torso.

TABLE I
pH, Osmolality, and Conductivity (κ) of Gastric Fluid, Various Foods, and Different Human Tissues at 37 °C

Fluid	**pH** [20], [21]	**Osmolality (mosm/kg)** [20], [21]	κ^{b} **(mS/cm)**
Human gastric fluid, fasted state[a]	1.5–7	191	6–17
Tap water	5.7–7.4	2–40	0.1
Orange juice	3.75	594–622	5.3
Coca Cola	2.4	493–695	1.4
Milk (2% fat)	6.73	271–282	6.3
Coffee	5.14	58	4.5

Tissue	κ**(mS/cm)**[22]
Fat, Lung, Spleen, Bone	0.0625–0.1
Lung, Liver, stomach, kidney, muscle (noncardiac)	0.667–1.49
Cardiac muscle (parallel, transverse)	7.604, 1.319

[a]Typical human gastric fluid composition [16–19]: Typical concentrations: Chloride (102±28 mM), Sodium (68±29 mM),Potassium (13.4±3 mM), Pepsin (1 mg/mL).
[b] Measured according to the Materials and Methods section.

with two conductivity domains [13]:

$$\mathrm{V} = 3\alpha I d \cos\theta / 4\pi \kappa_{\mathrm{outer}} R_{\mathrm{outer}}^2 \tag{7}$$

where $\alpha = 3/\{2 + \kappa_{\mathrm{inner}}/\kappa_{\mathrm{outer}} + 2\,(\kappa_{\mathrm{inner}}/\kappa_{\mathrm{outer}} - 1)\,(R_{\mathrm{inner}}/R_{\mathrm{outer}})^3\}$.

Equation (7) shows that the detected signal depends on the ratio between the inner and outer-domain conductivities. When the inner region is small and has a significantly higher conductivity, (7) provides up to a 3× increase in signal over the homogeneous case (5). In effect, the device's current and power are concentrated within the small high-conductivity region (the stomach) instead of being spread over the entire body. The low conductivity tissue outside the stomach behaves like a high impedance probe, allowing the electrical signal to be detected at the skin surface without drawing significant current.

For a nonspherical geometry, these effects are best seen with finite element simulations (see Fig. 5). The body can be modeled as a stomach with a conductivity of 7 mS/cm, surrounded by tissue with a uniform conductivity of 0.7 mS/cm. While this simplified model does not account for the heterogeneity and anisotropy of tissue, it in fact predicts the correct magnitude of the detected voltages on the skin compared to clinical results (10–100 μV, Fig. 7). For a sensor situated at the closest possible point relative to a receiver with 6-cm probe spacing, the simulations predict a detected signal of 150 μV. This is in fact very close to the value observed in clinical studies, as described later.

The finite element simulations are also useful for examining the potential due to the sensor throughout the body. The enhancement in signal due to the difference in stomach and torso

conductivity can be seen in Fig. 5(b), for the case of a theoretical "probe" as it is moved away from the sensor. The simulations show that the potential due to the sensor drops off very rapidly with distance; outside a distance of $\sim$2 cm [Fig. 5(a)], all voltages are within $\pm$5 mV of each other and the center of the sensor (used as the arbitrary ground reference). This is an important result as it indicates that the maximum voltage that the sensor can exert outside its immediate vicinity is $\sim$10 mV, far below the levels that would stimulate tissue or interfere with implantable devices such as pacemakers.

Equations (5)–(7) and the finite element simulations also predict a cosine dependence between the signal strength and the angle between the device and the receiver. This is verified in isotropic benchtop experiments [Fig. 4(b)]. The angular dependence was of some concern in the early stages of development as it implies that some devices in the stomach may be perfectly "misaligned" relative to the receiver and become undetectable. We have not found this "null" condition during preclinical and clinical testing, perhaps because of the conductive anisotropy present in human anatomy. Thus, such misalignment occurs over the life of a sensor less than 1% of the time. This is because the stomach and torso are highly heterogeneous media, providing multiple tortuous paths for the electric field to reach the receiver. Furthermore, over the typical *in-vivo* transmission time (several minutes), the sensor and receiver move relative to each other due to the peristaltic action of gastric waves and respiration. Thus, while the signal may be weak for certain periods of time, the probability of the sensor remaining perfectly misaligned relative to the receiver for the entire duration of communication is small.

Two additional aspects of the sensor design and signal propagation are worth noting. First, the physical parameters of the sensor can be traded off against each other to maintain or increase signal strength. For example, it may be desirable to reduce the size of the sensor and skirt to accommodate tablets or capsules whose smallest dimension is below 5 mm. This can be achieved without affecting the sensor's detection ability by increasing the output current of the sensor or increasing the receiver dipole length.

Second, the sensor has been specifically designed to provide a detectable signal while maintaining the simplest possible physical design. This is important for low cost, high volume manufacturing. The features that enable scalable manufacturing are the use of the skirt to enhance the sensor signal—eliminating the need for extended antennas and off-chip connections—and the integration of multiple functions into the same pair of electrodes on the device, which simultaneously provide for activation, power generation, and signal transmission. While this requires a high level of sophistication in the integrated circuit design, it ensures that the device can be made with a highly scalable manufacturing process.

III. Experimental Methods

A. Benchtop Testing

Test solutions were placed in a water-jacketed beaker maintained at 37+/−1 °C. The sensor was immersed and held in a fixed location at the center of the beaker using customized tweezers. The signal generated by the sensor was measured with two stainless steel electrodes, symmetrically located at a fixed distance from the device [see Fig. 3(d)] and connected to a high speed data acquisition system for measuring and decoding the signal. The currents shown in Fig. 3(a) and (b) were obtained using metal pincers to connect sensors to an oscilloscope and the current flow was determined by measuring the voltage across a known resistor. Solution conductivities were measured with a Hach Sension 5 conductivity meter.

B. Safety Studies

1) Chemical Extraction Studies: Sensors were incubated in deionized water adjusted to pH 1.2 and pH 7 with HCl or phosphate buffer to simulate gastric and intestinal conditions. Incubations were performed for 72 h at 37 °C with gentle agitation. Extraction ratios were selected per the ISO-10993-12 standard [14]. The extracts were tested using Inductively-Coupled Plasma Mass Spectroscopy to quantify inorganic compounds and Gas Chromatography-Mass Spectrometry to quantify organic compounds.

2) Toxicology: Repeat dose study in canines—the canine study was a 7-day, repeat-dose oral toxicology study. The test articles were complete devices placed in gelatin capsules prior to dosing. Twelve beagle dogs ($n = 4$ in the $1\times$ group, $n = 4$ in the $2\times$ group, and $n = 4$ controls) were used in this study. The daily dosage for the $1\times$ and $2\times$ dosing groups 24 and 48 devices per day, respectively. Daily clinical observations were performed during dosing, and whole blood was drawn from each animal at Day 0 and Day 7. Inductively coupled plasma-mass spectrometry (ICP-MS) was used for the quantification of materials in the blood. Animals were sacrificed on Day 7 for gross pathological analysis, organ weights, and histological analysis of gastrointestinal tract tissues.

Oral gavage in rats—sensors were incubated for 4 h at 37 °C in simulated gastric fluid (0.15 M NaCl solution, buffered to pH 1.8 + 1.0% pepsin), followed by simulated intestinal fluid (0.15 M NaCl, buffered to pH 7.0 + 0.035% bile salts + 0.035% pancreatin) for 68 h. The extraction ratio was selected per the ISO-10993-12 standard [14]. Eighty-four Sprague–Dawley rats were divided evenly into seven dosing groups: two control groups (water and extraction vehicle groups) and $0.33\times$, $1\times$, $10\times$, $100\times$, and $1000\times$ groups. The $1\times$ group represented the weight-adjusted rat equivalent to 30 sensors ingested simultaneously on a daily basis by a human. Animals received a single, daily oral gavage dose for 14 days, using a constant dose volume of 10 mL fluid/kg body weight. Regular clinical observations, including exams, mortality/moribundity checks, body weights, food consumption, and ophthalmoscopy, were performed. Blood counts, biochemistries, and coagulation were obtained under anesthesia on Day 14. Thereafter, animals were sacrificed for gross necropsy, organ weights, and histopathological analysis of a broad set of tissues commonly examined in dose-response toxicology studies.

C. Mechanical Safety

Assessment of luminal injury–sensors were prepared incorporating a thin layer of tantalum to ensure radiopacity on digital radiographs. Four canines (two in the experimental group, one positive control, and one negative control) were used. Sensors were administered in gelatin capsules to the experimental animals (50 devices each) and the positive control animal (10 devices). The negative control group received ten cellulosic discs without microchips. Serial digital radiographs, obtained at $t = 0$, $t = 3$ h, $t = 24$ h, and $t = 72$ h, were interpreted independently by two veterinary radiologists, who had been provided with *in-vitro* images of sensors in various orientations.

Assessment of transit time—sensors labeled with tantalum as above were administered in gelatin capsules to the experimental group (two animals, given 50 sensors each) and the positive control group (one animal, ten ingestible sensors). For the negative control group (one animal), ten cellulosic discs without microchips were administered. Serial digital radiographs, obtained at $t = 0$, $t = 3$ h, $t = 24$ h, and $t = 72$ h, were interpreted independently by two veterinary radiologists, who had been provided with *in-vitro* images of sensors in various orientations.

D. Electrical Safety

Assessment of cardiac dysrhythmia—two canine subjects were used to test the effect of typical and exaggerated sensor pulses delivered from the esophagus—the location in closest proximity to the heart. An electrophysiology (EP) catheter was used to deliver pulses at two locations in the esophagus: 1) at the point of maximal mechanical cardiac impact, visualized in the esophagus with an endoscope and 2) at the point where the highest amplitude transesophageal electrogram was measured. A signal generator produced simulated sensor signals, with frequencies ranging from 3 to 100 kHz and a maximum amplitude of 10 V ($>6\times$ the maximal voltage produced by the sensor), each delivered for 2 min. During pulse delivery, surface ECG traces were continuously monitored.

Assessment of electrochemical injury—an endoscope was used to visualize the gastric mucosa to identify pristine tissue suitable for a test location in a canine model. A custom-made pulse delivery paddle, incorporating the sensor's anode and cathode materials, was inserted and apposed to the stomach wall with the help of suction capability built into the periphery of the device. Electrical pulses of nominal and exaggerated strength were delivered to the test location. This included signals with a carrier frequency of 10 kHz as well as direct current, at current of $\leq$10 mA delivered for 1 min. Each test location was marked using suction and electrocautery. This pulse delivery method was repeated on the stomach and the esophagus endoscopically, and again on the stomach via a gastrostomy. After the animal was sacrificed, gross necropsy and histologic analysis were performed.

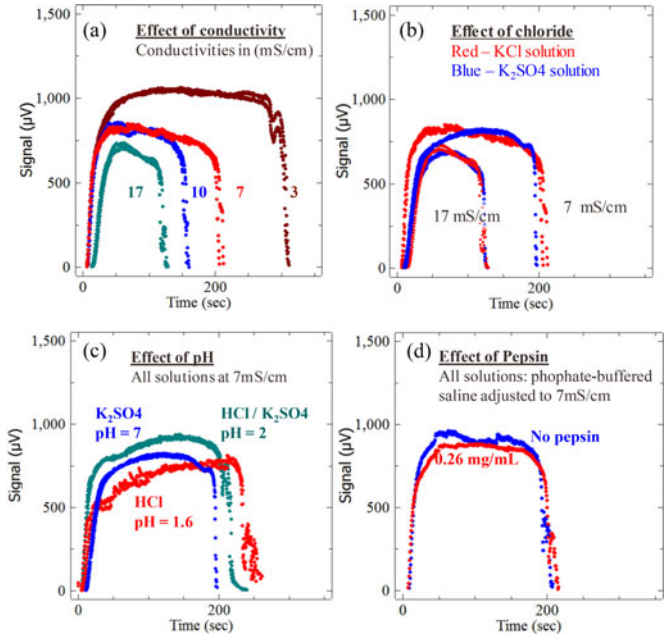

Fig. 6 Effect of (a) conductivity (KCl solutions) (b) chloride concentration (0 and 130 mM) (c) pH, and (d) pepsin concentration on discharge profiles. All testing was done at 37 °C.

E. Clinical Studies

The clinical studies were observational prospective studies conducted in healthy volunteers or specific patient populations. In each study, patients wearing a receiver were asked to ingest devices integrated into a suitable dose form to evaluate system performance and safety. Directly observed ingestion was used as a comparator to assess system performance, with the performance primary—positive detection accuracy—defined as the number of detected devices divided by the number of ingested devices. Further details are described in [15].

IV. Results

A. Performance in Biological Fluids

The stomach is a complex and variable chemical environment. Upon ingestion, food or medication is mixed with saliva and the basal stomach contents. The secretion of acid, electrolytes, enzymes, and surfactants modifies this mixture soon after ingestion, as do the slower processes of dissolution, digestion, and gastric emptying. Further variations may occur due to differences in patient physiology and medication, such as the use of proton pump inhibitors.

A series of *in vitro* tests were performed to assess the sensor's ability to function over the range of conditions created by these phenomena. Test solutions were selected based on the ranges of pH, conductivity, and enzyme and surfactant concentrations reported in the literature or measured *in vitro.*

The most critical property of stomach fluid is its conductivity. This is shown in Fig. 6(a) with KCl solutions at 3, 7, 10, and 17 mS/cm conductivity (all at 37 °C). Changing solution conductivity results in a proportionate decrease in discharge lifetime

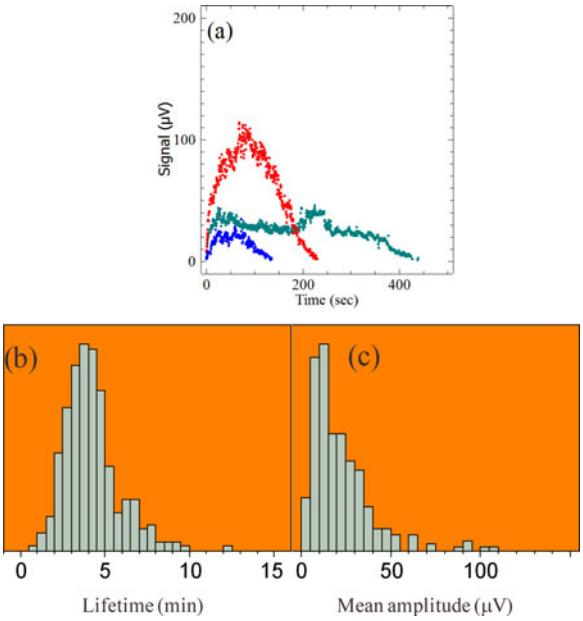

Fig. 7 Typical *in-vivo* discharge profiles for three ingestible sensors (a–b) and histograms of device lifetimes (b) and mean amplitude (c) from a representative clinical study.

due to the change in the sensor's impedance and output current. Over the wide range of conductivities shown in Fig. 6(a), the device runs for 120–400 s. *In vivo* discharge lifetimes vary over a comparable range. The minimum time needed for successful detection is about 5 s, so that the discharge times shown in Fig. 6(a) represent significant margin above the level necessary for successful detection.

The effects of other parameters—chloride, pH, and pepsin are shown in Fig. 6(c) and (d). Only pH has a noticeable effect. Changing pH from 1.6 to 7 (a change of five orders of magnitude in H^+ concentration) at a constant conductivity produces very little change.

The effects seen in Fig. 6 are best understood in the context of reactions (1)–(4). The reactants required by the main electrode reactions are copper and magnesium, both of which are supplied by the device itself. The only essential component provided by the stomach fluid is a medium with sufficient ionic conductivity to complete the circuit and reactions. The minor effect of pH is through side reaction (4). Lower pH increases the rate of the side reaction and increases the solubility of the $Mg(OH)_2$ byproduct; the two effects partially compensate for each other, resulting in a modest effect. The other species do not participate as reactants and have little impact on the kinetics of the electrode reactions.

B. Device Safety

Safety considerations were an essential part of the sensor design. As a mucosal contacting device, the Ingestible Sensor was evaluated according to the framework defined by the *ISO-10993 International Standard for Biological evaluation of Medical Devices* [14]. The key studies used to assess chemical, toxicological, mechanical, and electrical safety are listed in Table II.

TABLE II
KEY SAFETY STUDIES

Category	Purpose	Model
Chemical safety	-Quantify extractable species, simulated gastric / intestinal fluids	None
Toxicology	-Dose response (24 or 48 devices per day, 7 days)	Canine Rodent
	-High-dose oral gavage (up to 33,000 devices per day on a body-weight adjusted basis, 14 days)	
Mechanical safety	-Gastric transit time	Canine
	-Luminal injury	Canine
Electrical safety	-Cardiac stimulation / dysrhythmia	Canine
	-Electrochemical injury to GI lumen	Canine

1) Chemical Safety and Toxicology: The Ingestible sensor is comprised of an integrated circuit (0.85 mg, primarily silicon), the two active layers (CuCl (0.02 mg), and Mg (0.015 mg), and excipient materials that make up the insulating skirt disk and adhesive layer used to attach the IC to the skirt (ethyl cellulose, hydroxypropyl cellulose, and triethyl citrate). The total weight of the device is 7.1 mg.

According to the ISO-10993 guideline, the Ingestible Sensor is a mucosal contacting device. However, since the device is designed to elute species like copper and magnesium ions during operation, the levels of material released by the device were assessed using the International Conference on Harmonisation's standard for reporting and qualifying impurities in a new drug substance [23]. From this perspective, the ingestible sensor is viewed as another component of a pharmaceutical dose form, and any materials released by the device in the body are viewed as "impurities."

In the first phase, the quantities of all species or impurities released by the sensor in the gastrointestinal tract were established using *in-vitro* extraction studies. Extractions were performed on devices incubated in pH 1.2 or pH 7 media for 72 h at 37 °C to represent both low- and high-pH gastric environments. The media consisted of deionized water and hydrochloric acid or phosphate buffer. No surfactant or enzyme was added to the media to avoid introduction of extraneous species and impurities during analysis. Inorganic and organic species were quantified using ICP-MS and GC-MS, respectively. The species detected above the reporting threshold of 0.05% of device weight (the criteria established by the ICH [23] for a new drug substance) are shown in Table III. These consist of copper and magnesium ions, ethyl citrate, and various fragments of cellulose polymers.

The safety of each of these components was evaluated related to established ingestion guidelines (see Table III), typically expressed as a recommended daily average (RDA) or acceptable daily intake (ADI) for each material. For copper and magnesium, the detected levels are 125× [24] and 53 000X [25] below the recommended daily intakes of each species. Similarly, the level of ethyl citrate was 4600× below the established acceptable daily limit [26]. A variety of peaks in the GC-MS spectrogram

TABLE III
MATERIALS DETECTED IN EXTRACTION STUDIES COMPARED TO NUTRITIONAL GUIDELINES

Element	mg/device pH 1.2	pH 7	ADI or RDA (mg/day)
Copper	.0071	0.0002	0.9 [24]
Magnesium	.0079	.0070	420 [25]
Ethyl citrate	0.263	0.231	1200 [26]
Cellulose	Not quantified	Not quantified	Laxative effect at 5–30 g/day

were identified as cellulose fragments due to HPC and EC but were not quantified due to the large number of fragments. This is as expected given the high molecular weight and polydispersity of the cellulosic polymers used in the skirt. These cellulose derivatives are widely used as pharmaceutical excipients and food additives. The Joint FAO/WHO Expert Committee on Food Additives [27] has specified that these additives may be included in food products with no upper limit, since they are essentially dietary fiber materials. The only recommendation regarding ingestion levels is a precaution regarding laxative effects, which occur at 5–30 g/day [27]; the quantities used in Ingestible Sensor are three orders of magnitude below this range.

In the second phase, two toxicological studies were performed to further assess device safety by administering sensors or concentrated sensor extracts to animal models. In the first toxicological study, daily doses of 24 or 48 devices were administered to 12 canines for seven consecutive days. Blood samples were analyzed on days 0 and 7 and showed no differences in the levels of materials between test and control groups or between pre- and post-7-day-dosing states. No significant differences were found at these dose levels in terms of clinical observations, bodyweights, and food consumption. At the end of the 7 day period, gross organ pathology, organ weights, and microscopic analysis of selected gastrointestinal tissues and liver were performed and also indicated no difference between control and test groups.

A second toxicological study was performed using oral gavage in Sprague–Dawley rats to test dose response at even higher dose levels. Sprague–Dawley rats were selected because they have no vagal response to ingestion of relatively high concentration copper solutions. Solution extracts were obtained by incubating devices in simulated gastric fluid (4 h) followed by simulated intestinal fluids (68 h). Doses of 0, 0.7, 2.1, 21, 214, and 2143 mg/kg body weight/day were administered daily for 14 days using oral gavage. On a body-weight adjusted basis, these correspond to ingestion of 0, 11, 33, 330, 3300, 33 000 devices a day for 14 days in a 70-kg human subject. Animals were examined daily for mortality/moribundity, body weight, food consumption, and ophthalmoscopy. At the end of the study, subjects were evaluated for the evidence of toxicity in terms of blood counts, biochemistry, and coagulation, gross necropsy, organ weight, and tissue histopathology. The results showed no evidence of sensor-related toxicity, even in the highest dosing group. There were no differences between the control groups and the treatment groups with regard to clinical observations and histopathology. A statistically significant increase in thyroid gland weight was observed in the male subjects at dosing levels of 2.1 mg/kg body weight/day or greater. The increase was not correlated to dosing level and not observed in any of the female dose groups. No histological correlation was found between thyroid weight increase and examination of liver or pituitary gland tissue, which are typically associated with thyroid function. Therefore, this difference was considered unrelated to sensor exposure. Given the lack of toxicity, a NOAEL (no observable adverse effect level) could not be established.

2) Mechanical Safety: The sensor consists of an insoluble portion—the integrated circuit—equivalent in size to a food particle—and a cellulosic disk comprised of insoluble (ethyl cellulose) and soluble components (hydroxypropyl cellulose and triethyl citrate). The skirt becomes mechanically soft after immersion in gastrointestinal fluids. The sensor is therefore expected to be mechanically handled by the gut like a food particle or incidentally ingested grain of sand.

To confirm this, two animal experiments were performed to assess gastric transit time and any potential risk for luminal injury. In the first experiment (luminal injury), 40 sensors were administered per day for three days to canine subjects (two test subjects, one control subject). Stool frequency, character, and hemoccult were checked for three days prior to dosing and during dosing. No changes were observed in any of the stool parameters. Gross necropsy following day 3 and examination of the gastrointestinal tract in its entirety revealed no evidence of any mechanical injury.

In the second experiment (gastrointestinal transit time), canines were given 50 devices (experimental group, two animals), ten devices (positive control group, one animal), or ten skirts with no IC (negative control group, one animal). The devices were labeled with radiopaque tags and each animal was imaged via X-ray at $t = 0, 3, 24, \text{and } 72$ h. At $t = 0$ and $t = 3$ h, ten devices were identified as expected in the positive control animal. Multiple devices (nonquantified by design) were identified in the experimental animals. At $t = 24$ h, devices were visualized in only one experimental animal, and by $t = 72$ h, no devices were visualized in any animal, indicating transit and excretion of all devices. No devices were visualized at any of the time points in the negative control animal. These results confirmed that the device transits through the GI tract on a time scale comparable to the transit times for foods and small particles in humans and canines [17], [28]–[30].

We note also that the mechanical tests described earlier were conducted with an earlier generation of the sensor than the one shown in Fig. 2. This version of the sensor contained an integrated circuit with a higher thickness -0.45 mm instead of 0.3 mm. This was because at the time of the study, the IC was manufactured with an earlier version of the manufacturing process. The surface dimensions of the IC and amounts of active materials were otherwise identical. The success of the mechanical tests with the larger version of the IC provides further confidence in the mechanical safety of the final design.

3) Electrical Safety: Electrical safety was evaluated with regards to three potential mechanisms: 1) stimulation of cardiac or gastrointestinal tissue, 2) interference with implanted medical devices such as pacemakers and defibrillators, and 3) luminal

injury to the gastrointestinal tract due to the electrochemical reactions occurring at the electrodes. All three risks are low, as the sensor outputs a maximum voltage of only 1.85 V at open circuit with very short pulses of 5 to 50 μs. Furthermore, the voltage due to the sensor drops off as the square of the distance from the device, so that outside a 1–2 cm volume, all voltages are between -5 and $+5$ mV and the maximum voltage available to stimulate tissue is at most 10 mV (see Fig. 5).

To assess the possibility of cardiac stimulation, a canine study was performed using two canine subjects. An electrophysiology (EP) catheter delivered representative and exaggerated pulses at two different locations in the esophagus, the section of the GI tract where the sensor would be in closest proximity to the heart. The two locations stimulated were 1) the point of maximal mechanical cardiac impact, visualized in the esophagus with an endoscope and 2) the point where the highest amplitude transesophageal electrogram could be measured. A signal generator produced simulated electrical pulses, with carrier frequencies ranging from 3 to 100 kHz and a maximum amplitude of 10 V ($>6\times$ the maximum open circuit voltage produced by the sensor), each delivered for 2 min. During pulse delivery, surface ECG traces were continuously monitored. No ECG abnormalities were observed in either animal, confirming the initial assessment that there is no practical risk of cardiac stimulation.

To put this in further context, many literature studies have evaluated the magnitude and frequency of electrical signal required to stimulate cardiac tissue. These results are usually presented as strength-duration curves [31], [32] and show that with a shorter pulse, a higher value of current or voltage is required to elicit a response. At the pulse width characteristic of the sensor (5 to 50 μs), a current of 5.5–50 mA would have to reach the heart to elicit a response. This is virtually impossible since the current generated by the sensor has a peak value of $\sim$1–2 mA and the voltage due to the sensor is almost entirely confined to the high conductivity stomach environment.

Strength-duration curves are not readily available for gastrointestinal tissue. A number of recent studies have successfully utilized electrical signals to modulate gastric slow waves or improve clinical symptoms associated with gastroparesis [33]–[35]. The voltages and pulse widths needed to elicit a response in these studies are significantly larger than those generated by the sensor. In one study [35], electrodes implanted 2–3 cm apart on the mucosal side of the gastric lining were unable to generate any response with pulses of up to 10 V and 330 μs pulse width. Thus, the ingestible sensor operates in a regime with essentially no risk of tissue stimulation.

The final part of the electrical safety evaluation was addressing the risk of chemical burns due to species generated at the sensor electrodes. Chemical burns due to implanted electrodes are typically due to electrochemical reactions that break down water and drive the local pH to very high (pH $>$ 12) or very low values [36]. Due to its relatively low operating voltage, the sensor does not possess sufficient power to drive water electrolysis at an appreciable rate. The main chemical burn risk is due to side reaction (4), which consumes acid and produces $Mg(OH)_2$, thereby raising the local pH. The maximum pH change is set by the solubility product of $Mg(OH)_2$ ($1.5e^{-11} mol^3/L^3$) which sets a maximum pH of 10.5 in a saturated Mg^{2+} solution. This value is $\sim 5\times$ lower than that needed to cause injury. Furthermore, electrochemical lesion formation is most probable when there is a prolonged electrode-tissue contact. For the ingestible sensor, the tissue contact duration is likely to be short and variable as stomach peristalsis will constantly turn the device and propel it forward.

To confirm the low risk of electrochemical injury, a canine study was performed. An endoscope was used to visualize the gastric mucosa to identify pristine tissue suitable for a test location. A custom-made pulse delivery paddle, incorporating the same anode and cathode materials as the sensor, was inserted and apposed to the stomach wall, with the help of suction capability built into the periphery of the device. Electrical pulses of nominal and exaggerated strength were delivered to the test location. This included signals identical to the sensor with a carrier frequency of 10 kHz as well as direct current, at current of up 10 mA delivered for 1 min. Each test location was marked using suction and electrocautery. This pulse delivery method was repeated on the stomach and the esophagus endoscopically, and again on the stomach via a gastrostomy. After the animal was euthanized, gross necropsy and histologic analysis were performed. No evidence of pulse-related injury was detected, supporting the assessment of negligible risk of electrochemical injury from the sensor.

C. Pharmaceutical Integration

The ingestible sensor is intended to be integrated with a pharmaceutical oral dose form (tablet or capsule). This can be accomplished via one of three approaches during pharmaceutical manufacturing. The device can be incorporated into a tablet during tablet compression, placed inside a hard gelatin capsule during capsule filling, or attached to the surface of a tablet or capsule using an edible adhesive layer.

All three approaches have been successfully demonstrated via benchtop, preclinical, and clinical studies. In all cases, the combined dose form must meet the requirements of the pharmaceutical product—drug assay and effective release (typically evaluated via dissolution testing), stability, visual appeal, and physical integrity—while providing a suitable vehicle for delivery and activation of the sensor. The approaches and relevant case studies are presented in detail elsewhere [37], [38].

D. Clinical Performance

The ingestible sensor was evaluated in a series of clinical trials involving healthy volunteers or patients in specific therapeutic areas, including those with hypertension, heart failure, diabetes mellitus, tuberculosis, bipolar affective disorder, and schizophrenia (see Table IV). Testing was performed in adults with body mass index ranging from 16.0 to 56.8 kg/m^2. The therapeutic areas selected were those where a compelling need exists for a networked system to measure medication adherence and complementary physiologic metrics. In each trial, the sensor was tested as part of a complete system, consisting of the sensor integrated with a suitable dose form (tablet or capsule),

TABLE IV
EXPOSURE AND PERFORMANCE IN CLINICAL TRIALS

412 subjects	99.1% Detection accuracy
20,993 ingestions	100% Correct identification
Maximum daily ingestion: 34	0% False positives
Maximum use days: 90 days	No SAEs / UADEs related to system

Trials were conducted in the following patient populations. The number of patients in each study is indicated in parentheses: Healthy Volunteers (296), Cardiovascular disease (53), Tuberculosis (30), Psychiatry (28). SAE = Serious Adverse Event; UADE = Unanticipated Adverse Device Effect).

a receiver unit worn by the patient, and a device for interfacing with the system (typically a cell phone with a graphical user interface). Physiologic metrics such as heart rate, blood pressure, activity, and sleep quality were measured and compared with adherence patterns to provide a continuous, real-time picture of a patient's health. The designs and results of individual clinical trials have been reported elsewhere [15], [37], [38]. Here, we focus on the aggregate performance of the ingestible sensor across all trials (see Table IV).

The primary measure of sensor performance *in vivo* is the positive detection accuracy (PDA). PDA is defined as the percentage of detected devices that have been administered under direct observation. The most recent confirmatory study of performance, which tested the latest configuration of the system, demonstrated a PDA of 99.1% (321 detected/324 ingested under direct observation, 95% CI 97.3%–99.7%).

The 0.9% of devices that went undetected represent contributions from all components of the system. For the sensor, the most likely contribution is due to physiological corner cases, where a combination of stomach environment and receiver–sensor orientation may result in a small proportion of devices (no greater than 0.9%) being missed.

Fig. 7(a) shows typical *in-vivo* signals from several sensors ingested by healthy volunteers. Sensors were compressed inside nonactive tablets for this study. The difference in duration of discharge of the devices shown is due to differences in local stomach conductivity and device impedance. The signal strengths are different because the local environment, sensor position, and orientation are free to vary with time; the discrete amplitude changes within each device are most likely due to sensor movement, whereas differences in chemical environment occur on a slower time scale and are more likely to account for differences between sensors ingested at different times. Due to the characteristic drop off in electric potential as a function of distance from a dipole, signal strengths tend to be lower in subjects with larger BMI, but remain well above the receiver's detection threshold of 1 μV in subjects up to a BMI of 56.8 kg/m^2.

V. DISCUSSION

The results presented here demonstrate the safety and clinical performance of the ingestible sensor, the first instance of a microfabricated integrated circuit developed and approved for daily ingestion by patients. The sensor has been designed and optimized to measure ingestion events in a direct and accurate manner and allows direct correlation of medication adherence to other physiological metrics.

The first application of the ingestion sensor is to measure a patient's adherence to oral medication therapy regimens. By allowing direct and timely feedback to the patient and caregivers, the sensor provides a tool for improving adherence behavior. This can be done by sensing enough ingestion events to allow statistically meaningful determination of a pattern of behavior for a given patient. It is important to note that the detection accuracy of such events need not be perfect, rather only sufficient to provide a statistically meaningful classification of adherence behavior within a reasonable period of time. The higher the detection accuracy, the fewer ingestion events needed for such classification for a given statistical level of confidence. Beyond medication adherence, the sensor can also be combined with nutritional supplements and foods for applications such as optimization of athletic performance and diet management.

The sensor also represents a platform for a new category of highly integrated physiological sensors, combining the functions of power generation and communication in a small, safe, and inexpensive form factor. The power source—a partial battery that utilizes the gastric fluid as its electrolytic solution—eliminates the need for a bulky power source. The communication channel utilizes the same electrodes as the power source to transmit data, enabling reliable and private communication within the body between multiple devices.

Many applications are possible beyond the measurement of ingestion events. Foremost among these is the detection of clinically important chemical species, including gastric pH, blood, and enzymes. By modifying the amount of active material on the device, applying suitable coatings, and using triangulation methods, the device can be adapted to activate and sense in specific parts of the GI tract. Gastric transit times and gastrointestinal electric activity can also be measured. Since the electrical signal must pass through the torso to reach the receiver, it offers the possibility of measuring properties such as hydration and fat content. Finally, the availability of a proven and safe ingestible integrated circuit can enable a new generation of "smart" drug delivery dose forms, with the ability to generate very specialized drug release profiles, target specific locations, and respond to local sensing events.

ACKNOWLEDGMENT

The authors would like to thank their many colleagues at Proteus Digital Health who assisted with this work.

REFERENCES

[1] L. Osterberg and T. Blaschke, "Adherence to medication," *N. Eng. J. Med.*, vol. 353, no. 5, pp. 487–497, 2005.
[2] "Thinking outside the pillbox: A system-wide approach to improving patient medication adherence for chronic disease," New England Healthcare Institute, Cambridge, MA, USA, 2009.
[3] K. Nasseh, S. G. Frazee, J. Visaria, A. Vlahiotis, and Y. Tian, "Cost of medication nonadherence associated with diabetes, hypertension, and dyslipidemia," *Amer. J. Pharmacy Benefits*, vol. 4, no. 2, pp. 41–47, 2010.
[4] J. N. Rasmussen, A. Chong, and D. A. Alter, "Relationship between adherence to evidence-based pharmacotherapy and long-term mortality after acute myocardial infarction," *J. Amer. Med. Assoc.*, vol. 297, no. 2, pp. 177–186, 2007.

[5] R. Balkrishnan, "The importance of medication adherence in improving chronic disease-related outcomes: What we know and what we need to know further," *Med Care*, vol. 43, no. 5, pp. 517–520, 2005.
[6] "The use of medicines in the united states : Review of 2011," IMS Institute for HEalth Informatics, Parsippany, NJ, USA, 2012.
[7] *Evaluation of automatic class III designation (de Novo) for Proteus Personal Monitor Including Ingestion Event Marker—K113070*. Food and Drug Administration Health, Center for Device and Radiological Health, 2012.
[8] D. Linden and T. B. Reddy, *Handbook of Batteries*, 3rd ed. New York, NY, USA: McGraw-Hill, 2001.
[9] F. Sammoura, K. B. Lee, and L. Lin, "Water-activated disposable and long shelf life microbatteries," *Sens. Actuators A, Phys.*, vol. 111, no. 1, pp. 79–86, Mar. 2004.
[10] A. Heller, "Potentially implantable miniature batteries," *Anal. Bioanal. Chem.*, vol. 385, pp. 469–473, 2006.
[11] H. Jimbo and N. Miki, "Gastric-fluid-utilizing micro battery for micro medical devices," *Sens. Actuators B, Chem.*, vol. 134, no. 1, pp. 219–224, Aug. 2008.
[12] E. Frank, "Electric potential produced by two point current sources in a homogeneous conducting sphere," *J. Appl. Phys.*, vol. 23, no. 11, pp. 1225–1228, 1952.
[13] S. Rush and D. a Driscoll, "EEG electrode sensitivity—An application of reciprocity," *IEEE Trans. Biomed. Eng.*, vol. 16, no. 1, pp. 15–22, Jan. 1969.
[14] *Biological Evaluation of Medical Devices—Part 12: Sample Preparation and Reference Materials*, vol. 12. International Organization for Standardization ISO 10993-12, 2007.
[15] K. Y. Au-Yeung, G. D. Moon, T. L. Robertson, L. A. Dicarlo, M. S. Epstein, S. E. Weis, R. R. Reves, and G. Engel, "Early clinical experience with networked system for promoting patient self-management," *Amer. J. Managed Care*, vol. 17, no. 7, pp. e277–e287, Jan. 2011.
[16] S. J. Watson, R. H. Smallwood, B. H. Brown, P. Cherian, and K. D. Bardhan, "Determination of the relationship between the pH and conductivity of gastric juice," *Physiological Meas.*, vol. 17, no. 1, pp. 21–27, Feb. 1996.
[17] F. Kong and R. P. Singh, "Disintegration of solid foods in human stomach," *J. Food Sci.*, vol. 73, no. 5, pp. R67–R80, Jun. 2008.
[18] M. Vertzoni, J. Dressman, J. Butler, J. Hempenstall, and C. Reppas, "Simulation of fasting gastric conditions and its importance for the in vivo dissolution of lipophilic compounds," *Eur. J. Pharmaceutics Biopharmaceutics*, vol. 60, no. 3, pp. 413–417, Aug. 2005.
[19] A. Lindahl, A. Ungell, L. Knutson, and H. Lennernas, "Characterization of fluids from the stomach and proximal jejunum in men and women," *Pharmaceutical Res.*, vol. 14, no. 4, pp. 497–502, 1997.
[20] M. Feldman and C. Barnett, "Relationships between the acidity and osmolality of popular beverages and reported postprandial heartburn," *Gastroenterology*, vol. 108, no. 1, pp. 125–131, Jan. 1995.
[21] B. Büttel, M. Fuchs, and B. Holz, "Freezing point osmometry of milk to determine the additional water content–an issue in general quality control and German food regulation," *Chem. Central J.*, vol. 2, pp. 6–12, Jan. 2008.
[22] C. Ramon, Y. Wang, J. Haueisen, P. Schimpf, S. Jaruvatanadilok, and A. Ishimaru, "Effect of myocardial anisotropy on the torso current flow patterns, potentials and magnetic fields," *Phys. Med. Biol.*, vol. 45, pp. 1141–1150, 2000.
[23] *Guidance for Industry—Q3A Impurities in New Drug Substances.* Silver Spring, MD, USA: Food and Drug Administration, 2008.
[24] *Dietary Reference Intakes for Vitamin A, Vitamin K, Arsenic, Boron, Chromium, Copper, Iodine, Iron, Manganese, Molybdenum, Nickel, Silicon, Vanadium, and Zinc*. Washington, DC, USA: National Academy Press, 2001.
[25] *Dietary Reference Intakes for Calcium, Phosphorous, Magnesium, Vitamin D, and Fluoride*. Washington, DC, USA: National Academy Press, 1997.
[26] *WHO Food Additive Series 44 - Safety Evaluation of Certain Food Additives and Contaminants*. Geneva, Switzerland: WHO, 2000.
[27] *Thirty Fifth report of the joint FAO/WHO Expert Committee on Food Additives—Evaluation of certain food additives and contaminants*. Geneva, Switzerland: WHO Press, 1990.
[28] T. Kararli, "Comparison of the gastrointestinal anatomy, physiology, and biochemistry of humans and commonly used laboratory animals," *Biopharmaceutics Drug Disposition*, vol. 16, pp. 351–380, 1995.
[29] R. Khosla and S. S. Davis, "The effect of tablet size on the gastric emptying of non-disintegrating tablets," *Int. J. Pharmaceutics*, vol. 62, no. 2–3, pp. R9–R11, Jul. 1990.
[30] D. A. Adkin, S. S. Davisa, R. A. Sparrow, and I. R. Wildingb, "Colonic transit of different sized tablets in healthy subjects," *J. Controlled Release*, vol. 23, pp. 147–156, 1993.
[31] L. Geddes, "Chronaxie," *Australas. Phys. Eng. Sci. Med.*, vol. 22, no. 1, pp. 13–17, 1999.
[32] L. Geddes, "Accuracy limitations of chronaxie values," *IEEE Trans. Biomed. Eng.*, vol. 51, no. 1, pp. 176–181, Jan. 2004.
[33] J. Zhang and J. D. Z. Chen, "Systematic review: Applications and future of gastric electrical stimulation," *Alimentary Pharmacology Therapeutics*, vol. 24, no. 7, pp. 991–1002, Oct. 2006.
[34] G. Song, X. Hou, B. Yang, Y. Sun, J. Liu, W. Qian, and J. D. Z. Chen, "Efficacy and efficiency of gastric electrical stimulation with short pulses in the treatment of vasopressin-induced emetic responses in dogs," *Neurogastroenterology Motility*, vol. 18, no. 5, pp. 385–391, May 2006.
[35] A. Arriagada, A. S. Jurkov, E. Neshev, G. Muench, M. P. Mintchev, and C. N. Andrews, "Comparative gastric motility study of enterra^{TM} therapy and neural gastric electrical stimulation in an acute canine model," *Neurogastroenterology Motility*, vol. 23, no. 3, pp. 271–278, Mar. 2011.
[36] T. Litovitz, N. Whitaker, and L. Clark, "Preventing battery ingestions: An analysis of 8648 cases," *Pediatrics*, vol. 125, no. 6, pp. 1178–1183, Jun. 2010.
[37] K. Y. Au-Yeung, T. Robertson, H. Hafezi, G. Moon, L. DiCarlo, M. Zdeblick, and G. Savage, "A networked system for self-management of drug therapy and wellness," in *Proc. Wireless Health Conf.*, 2010, pp. 1–9.
[38] L. DiCarlo, G. Moon, A. Intondi, R. Duck, J. Frank, H. Hafazi, Y. Behzadi, T. Robertson, B. Costello, G. Savage, and M. Zdeblick, "A digital health solution for using and managing medications," *IEEE Pulse*, vol. 3, no. 5, pp. 23–26, Sep. 2012.

Authors' photographs and biographies not available at the time of publication.